ingegneria sismica
International Journal of Earthquake Engineering
Anno XLIII - Num. 1 - 2026

Research on Intelligent Inspection Integration Platform Development and Key Technologies for Gas Power Plants

Zhimin Cui[1,*]

[1] Guoneng Guohua (Beijing) Gas-Fired Cogeneration Power Co., Ltd., Beijing, 100025, China

SUMMARY: *In this paper, an investigation will be systematically made on the architecture design and core algorithm optimization of an intelligent inspection integration platform in order to meet the safety and smart O&M demands of gas power plants. YOLOv5 detection algorithm is upgraded by means of integrating the attention mechanism of CBAM, multi-scale feature extraction of BiFPN and Focal EIoU loss function for enhancing oil leakage detection performance. A combination of Comsol simulation of temperature field and infrared image processing with SVM classification method is used for steam leakage identification. Experiment results of both oil leakage and steam leakage under simulation conditions are reported to test the feasibility of the intelligent inspection integration platform proposed in this paper. It is found that with the application of the enhanced algorithm, the mean average precision of real oil leakage sample reaches 80.14%, which is 24.13 percentage points higher than that of baseline YOLOv5 detection algorithm. In addition, the steam leakage alarm rate is up to 99.13%.*

KEYWORDS: *gas power plant intelligent inspection; oil leakage; steam leakage; YOLOv5 algorithm; SVM classification*

1 Introduction

In recent years, the energy sector has moved steadily toward cleaner production, greater intelligence, and deeper integration with information technology [1]. As grid power technology continues to advance and network informatization becomes more widespread, gas power generation enterprises have entered a new stage of development. It is no longer limited to the intelligence or automation of discrete equipment, but a complete system covering all relevant aspects of power generation, transmission, distribution, substation, power consumption and dispatch [2-4]. With advancements in technology and the increase in voltages, the implementation of greater automation and intelligence into power plants is becoming more realistic than ever before, while the number of components, subsystems and branches under the equipment is increasing, the crosslinking method is more complex, and the number of to-be-observed items (instrumentation, cosmetic defects, etc.) is huge, and other new problems appear again [5-8]. The traditional gas power plant manual periodic inspection work intensity, low efficiency, and may lead to maintenance over or under maintenance, the process of personal safety hazards and other issues are gradually exposed, the traditional operation and maintenance methods and methods by a strong impact [9]. Gas power plant as the power generation link of smart grid, the first step of the complete system, is one of the important basic support points of smart grid construction [10]. Against such a backdrop, the construction of an effective

*cuizhimin1107@163.com
https://doi.org/10.65102/is2026480
Published: 30 April, 2026

intelligent inspection integration system within gas power plants is of great importance to the entire gas power generation industry.

Madejski et al [11] constructed a mathematical model of a gas power plant, input the site environmental conditions and thermal energy demand data into the model, and calculated the current thermal energy and power production, which was used for the monitoring and optimization of power and thermal energy production. Khalid et al. [12] used machine learning methods along with optimal sensor selection approaches for boiler water-cooled wall tube leakage detection in smart steam power generation plants, resulting in enhanced efficiencies and accuracies in detecting such leaks. Ma et al. [13] designed a cloud computing-based approach for the diagnosis and monitoring of gas turbine generator systems by integrating unsupervised learning models with cloud computing technologies, showcasing the potential to diagnose faults in gas turbines with accuracy levels between 60% to 80%. Akhtar et al [14] proposed high vibration diagnostics of gas turbines based on probe data (baud, track, and shaft centerline plots), which identified the that the root cause of the failure is resonance, and the intrinsic frequency of the casing can be improved by increasing the stiffness, which reduces the maximum vibration amplitude by 38%. Bunyan et al. [15] employed artificial intelligence methodologies for thermal condition monitoring and predictive maintenance of gas turbines. Machine learning, in this case, has the ability to classify the states of faults in gas turbines accurately, and the proposed predictive maintenance strategy is able to prolong the mechanical service life. However, the current intelligent inspection of gas power plants is limited to a single component and lacks systematic intelligent inspection.

This paper puts forward the design scheme of key technologies based on the development requirements of intelligent inspection integration platform for gas power plants. Improve the YOLOv5 algorithm to realize oil leakage detection of pipelines in key areas of the power plant. A module for the CBAM attention mechanism is added for the purpose of improving feature learning and extraction, and the bidirectional feature pyramid network is used for multi-level feature fusion. Focal EIoU Loss is selected as the loss function to optimize regression accuracy as well as enhance the stability of the model. Design the defect detection model of steam pipeline based on infrared thermography, and simulate the surface temperature field of steam pipeline using Comsol software. Propose the preprocessing method of infrared thermal imaging image, and select the support vector machine model for defect classification. Combined with fieldwork and historical operation data, the oil leakage detection data set of pipelines in gas power plants is constructed. The advantages of the YOLOv5 method can be demonstrated by comparison tests. Carry out steam leakage simulation experiments to analyze the applicability of infrared thermal imaging method in steam leakage detection.

2 Development and key technology design of intelligent inspection integration platform for gas power plants

2.1 Intelligent inspection integration platform program design

The operation of gas power plants involves a large number of high-temperature and high-pressure pipelines and key equipment, and once oil or steam leakage occurs, it may not only cause equipment damage and environmental pollution, but also threaten the safety of personnel and stable operation of the unit. Therefore, it is urgent to establish an efficient and reliable intelligent inspection integration platform.

The gas power plant intelligent inspection integration platform studied in this paper is mainly used for the daily inspection work of gas power plants, the platform as the field

inspection and background expert management side of the “intelligent transit body”, can effectively connect the field inspection work and background management platform as a whole, so that the gas power plant inspection work becomes integrated, thus It improves the intelligence and efficiency of inspection. Intelligent inspection integration platform contains fault diagnosis algorithms, data storage modules, etc., and can be called through the GPRS network management side of the advanced algorithms, data and other resources, to achieve the field inspection data analysis and processing functions, the analysis results can be uploaded in real time to the backstage management side, the application of the field can provide support and guidance for the standardization of work. In this paper, we will start from the functional requirements of the platform and complete the detailed design of the key technologies of the intelligent inspection integration platform.

2.2 Identifying oil leaks in critical areas of power plants based on improved YOLOv5 algorithm

2.2.1 Integration of CBAM attention mechanisms

Using CBAM attention mechanisms can weaken the effect of changes in the background on the detection result and enable the model to focus only on learning and extracting oil leakage features in pipelines. This is accomplished through obtaining oil leakage feature information with different resolution scales based on differences between different pixel categories, channel features, and contextual relations. CBAM structure is depicted in Fig. 1.

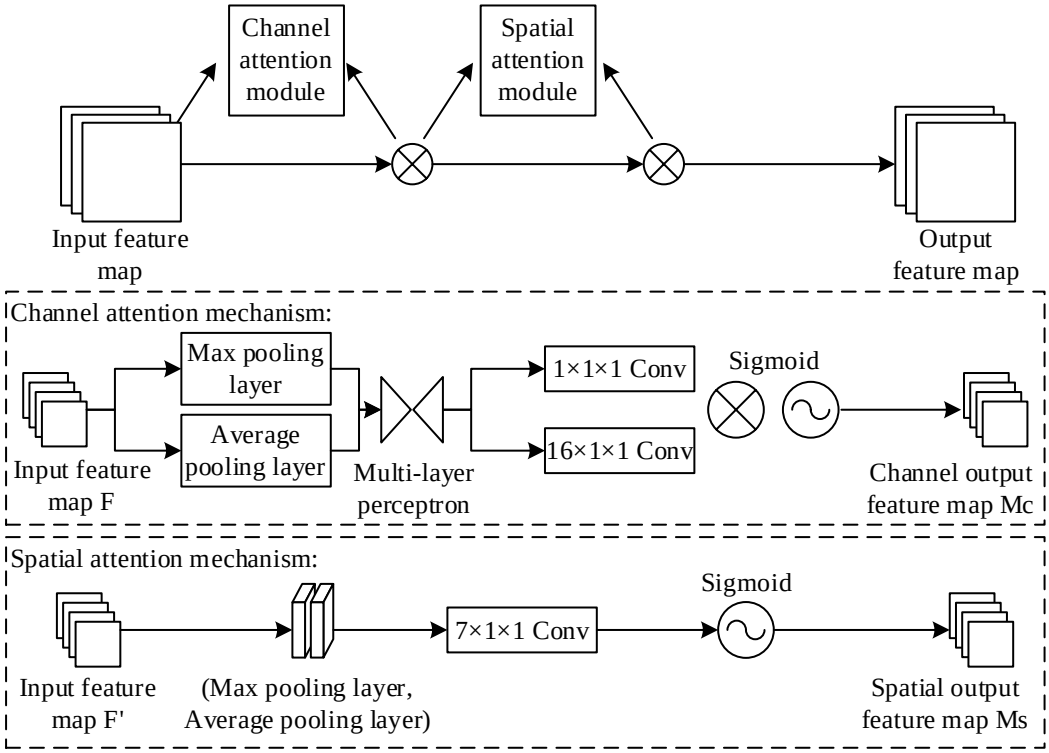

Figure 1: CBAM structure

CBAM attention mechanism is made up of two main components namely, channel attention component and spatial attention component. Both sub-components are independent of each other in the sense that each attends to attention operation either along channels or along space.

Redistribution of the weights in the channel attention module allows for more focus on critical features and less influence from irrelevant ones in the recognition results. The input feature maps are duplicated into two sets, where global maximum pooling and global average pooling are performed based on width and height to obtain two feature maps. They are then inputted into the MLP that contains two layers. After that, the obtained features are transferred to the spatial attention module.

The channel attention module output will act as the input in the spatial attention module. First, global max pooling and global average pooling will be done based on the channel to get two feature maps. Then, concatenation is performed on the channel dimension before being followed by a convolution process that results in one-channel output. Sigmoid activation is used to generate spatial attention features. In the end, multiplication will be carried out between the spatial attention features and the initial input features to get the feature map output of the CBAM attention model.

2.2.2 BiFPN-based multi-scale feature fusion network

In single-stage target detection algorithms, image features are extracted in one pass, which means feature information at different scales cannot be obtained directly. The features generated in the backbone segment are divided according to stage and denoted as $C1, C2, \cdots, C7$, where the number indicates how many times the image resolution has been halved. For example, C1 represents the first stage, whose output is a feature map at half the resolution of the original image, since the image resolution has been halved once. Feature fusion is then performed layer by layer from top to bottom, with the output denoted as P. The entire process can be expressed as Eq.

$$P_i, P_{i+1}, \cdots, P_{i+n} = f\left(C_i, C_{i+1}, \cdots, C_{i+n}\right) \tag{1}$$

The formula in Eq:

$C_i, C_{i+1}, \cdots, C_{i+n}$ -Generated features extracted in the i th stage;

$P_i, P_{i+1}, \cdots, P_{i+n}$ - the output of the i th stage;

F - the transformation process from input to output (including feature fusion between upper and lower layers);

The architectural structure of BiFPN is shown in Fig. 2. The key differences from PANet include:

(1) All nodes with entry degree 1 will be dropped because there is no more information to be added; they only add redundancy, as they carry the same information as the previous node.

(2) There are skip connections that ensure the information in the output layer comes from both the fused information at the bottom-up path and the information contained in the original nodes without fusion.

(3) The architecture is modularized, meaning that the whole architecture can be stacked for additional fusion. The relation between layers is described by equation(2).

$$\begin{cases} P_7^{out} = Conv(P_7^{in}) \\ P_6^{out} = Conv(P_6^{in} + \mathrm{Re}\,size(P_7^{out})) \\ P_5^{out} = Conv(P_5^{in} + \mathrm{Re}\,size(P_6^{out})) \\ P_4^{out} = Conv(P_4^{in} + \mathrm{Re}\,size(P_5^{out})) \\ P_3^{out} = Conv(P_3^{in} + \mathrm{Re}\,size(P_4^{out})) \end{cases} \tag{2}$$

The formula in Eq:

p^{in} - input features of the layer where it is located;

p^{out} - output features of the layer where it is located;

Resize -resolution matching operation for upsampling or downsampling;

Conv -convolution operation for feature processing;

With the substitution of path aggregation network of the original YOLOv5 algorithm with bidirectional feature pyramid network, the performance of detecting small objects is enhanced along with the reduction of computation resources utilized by the algorithm. Such an implementation holds great significance for the utilization of this technology in practical settings where processing power is limited.

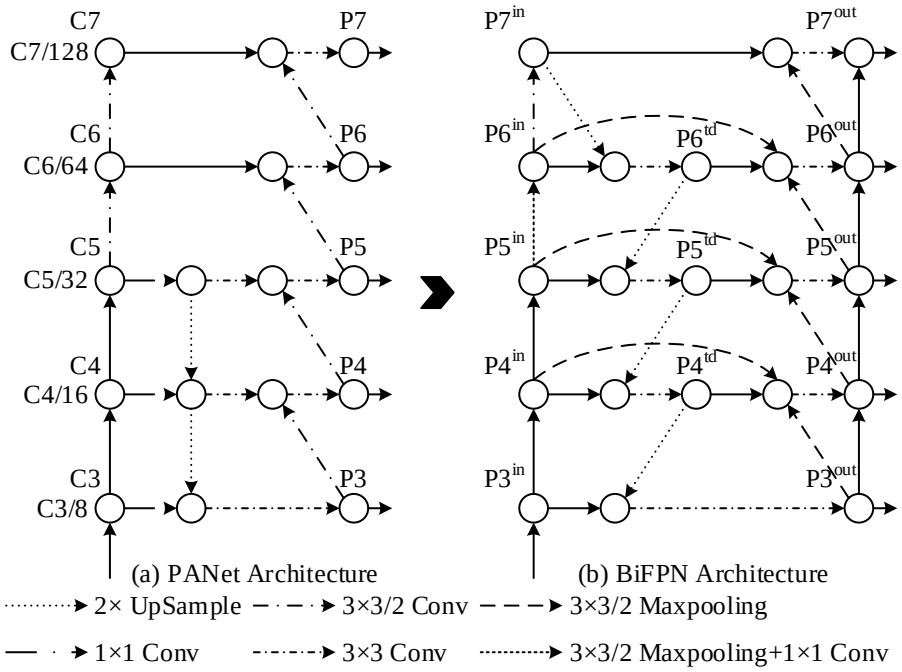

Figure 2: Overall structure of BiFPN

2.2.3 Focal EIoU Loss Loss Function

Loss function used in YOLOv5 is the CIoU Loss which has been improved from DIoU Loss by including an influence factor that takes into account centroid distance and aspect ratio. It is calculated as below:

$$CIoU\ Loss = 1 - CIoU \tag{3}$$

$$CIoU = IoU - \frac{Dis\tan ce_g^2}{Dis\tan ce_c^2} - \frac{v^2}{(1-IoU)+v} \tag{4}$$

$$v = \frac{4}{\pi^2}\left(\tan^{-1}\frac{w^{gt}}{h^{gt}} - \tan^{-1}\frac{w^{p}}{h^{p}}\right)^2 \tag{5}$$

Eq:

$Dis\tan ce_g^2$ is the distance between the center point of the prediction frame and the target frame;

$Dis\tan ce_c^2$ is the minimum outer rectangle diagonal length;

$\frac{w^{gt}}{h^{gt}}$ is the aspect ratio of the prediction frame;

$\frac{w^p}{h^p}$ is the aspect ratio of the target frame.

As opposed to DIoU Loss which takes into account centroid distance and aspect ratio, CIoU Loss is improved by the inclusion of an influence factor. However, the loss function fails to consider the aim of bounding box regression. This problem leads to poor and lengthy convergence in addition to imprecise regression results. In order to rectify this problem, the current algorithm has improved the previous CIoU Loss function (Eq. (3)) as seen in Eq. (6).

$$L_{Focal\ EIoU} = IoU^{\gamma} L_{EIoU} \tag{6}$$

Eq:

γ-hyperparameters used to control the curvature of the curve;

$EIoU$ divides the loss function into three parts: the IoU loss, the distance loss and the edge loss:

$$\begin{aligned} L_{EIoU} &= L_{IoU} + L_{dis} + L_{asp} \\ &= 1 - IoU + \frac{\rho^2(b, b^{gt})}{c^2} + \frac{\rho^2(w, w^{gt})}{c_w^2} + \frac{\rho^2(h, h^{gt})}{c_h^2} \end{aligned} \tag{7}$$

Eq:

L_{IoU} is the IoU loss;

L_{dis} is the distance loss;

L_{asp} is the edge loss;

c_w is the width of the minimum outer frame covering the prediction and target frames;

c_h is the height of the minimum outer bounding box covering the prediction and target boxes.

One unique feature about Focal in Focal EIoU Loss is that it is different from traditional Focal Loss because while traditional Focal Loss increases loss for harder samples to mine hard samples, in Focal EIoU Loss, loss increases according to a higher IoU. This brings a weighted effect where well-regressed targets receive more loss in order to improve the quality of regression.

Normalization through division of differences in width and height of predicted samples against the minimum outer bounding box enhances the speed and accuracy of regression. Using Focal Loss helps address the issue of sample imbalance in bounding box regression optimization. The method works by reducing the weight of anchor frames that have lower overlapping area with the target frames so as to focus on good anchor frames.

2.2.4 Backbone network design

From the perspective of practical computational overhead, a method of oil leakage detection in pipelines in critical regions of power plants is put forward based on YOLOv5, which is a modified model. The overall framework of CBAM-YOLOv5 is illustrated in Fig. 3.

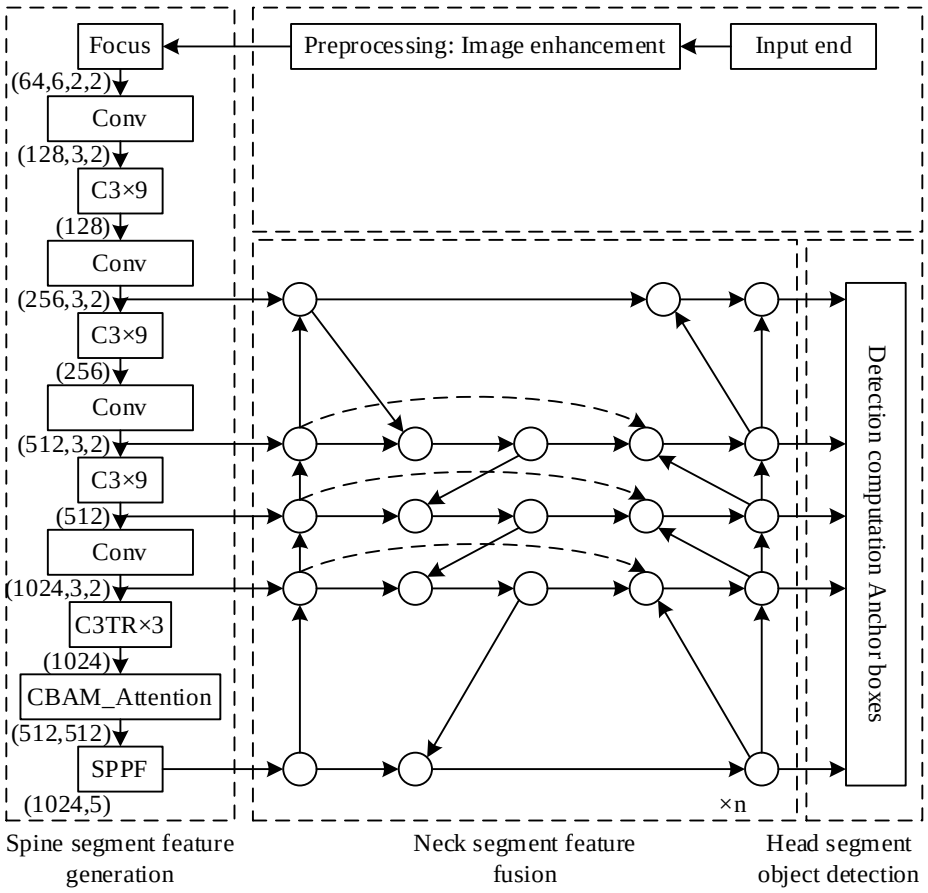

Figure 3: Overall structure of CBAM-YOLOv5 algorithm

In addition to adopting CBAM in the improved algorithm, the learning capability of regional features is enhanced, thus helping the model focus more on the extraction of useful information regarding oil leakage rather than being interfered by complicated backgrounds when making judgments. Due to the small size of leakage targets in the power plants' pipelines, a bi-directional feature pyramid network will be used for multiscale feature fusion and minimizing redundancy, thereby promoting the detection of small targets. In order to improve the detection accuracy, Focal EIoU Loss will be applied in this improved algorithm to guide the model towards quality anchor frames for faster convergence and better results.

2.3 Identifying steam leaks in critical areas of power plants based on infrared thermal imaging technology

2.3.1 Finite element simulation analysis

(1) Simulation Modeling and Solving

The Comsol Multiphysics software is an advanced multi-physics simulation software that can simultaneously take into consideration multiple physical fields such as thermal conduction,

fluid flow, and radiation and hence be able to provide accurate results in solving the equations governing these processes, thereby obtaining accurate distributions of the temperature fields. This study begins with the construction of a steam pipe model based on the actual parameters of the steam pipeline, setting up materials and parameters according to actual requirements. Then, the temperature field distribution of the external pipe layer is solved, and both the map of temperature field distribution and temperature variation curves are obtained for analysis of the surface temperature changes in the steam pipe. Based on the discussion of abnormal external temperature distribution caused by operation factors, defect models are built in steam pipes which may be encountered during practical operations, and a series of simulations are performed for the surface temperature fields of the pipeline with different operation situations. Figure 4 shows the process of simulation in particular cases.

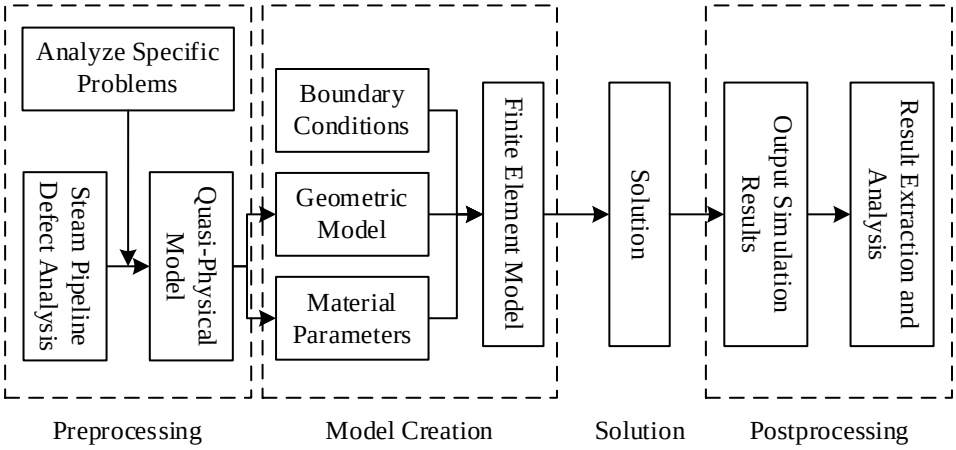

Figure 4: Simulation analysis process

(2) Geometric modeling

Geometric models are designed using two methods in Comsol 6.0. These methods include drawing of the geometric model directly in the program and importing of files created in CAD modeler. To help adjust parameters of the model, the steam pipe model will be created in this experiment using the Comsol program. It is done based on the size and specifications of the steam pipes that need to be inspected, and the created model is presented in Figure 5 below.

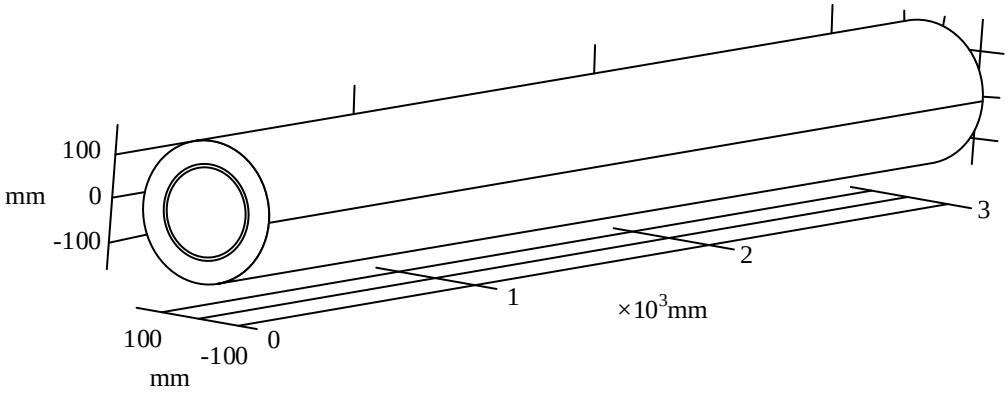

Figure 5: Steam pipe model

In the actual work of steam piping, most of the time is normal operation, so first establish the steam piping model under normal operation as a control. Over the course of time, steam

pipes tend to get affected by hole-type defects due to the occurrence of steam corrosion inside the pipes. As such, there will be variations in the temperatures of the surface of the pipes. Similarly, absence of an insulation layer or damage to the outer layer of tin coating of the steam pipe would equally contribute to changes in the surface temperature of the steam pipes. For the purpose of acquiring knowledge about the temperature field distributions in steam pipes, both the insulation layer and iron layer have been considered individually during simulations.

(3) Control equations and boundary conditions

During normal operation of a steam pipeline, the steam inside the pipeline can be considered as a viscous incompressible fluid. It can be calculated by the Navier-Stokes equations, the standard $k-\varepsilon$ turbulence model is chosen, and the coupled implicit steady state flow field calculation method is used.

The fluid governing equations and heat transfer equations, including the energy conservation equation, the continuity equation, the NS equation, and the differential equation of thermal conductivity are as follows:

Energy conservation equation:

$$\frac{\partial}{\partial t}(\rho T)+div(\rho(uT))=div\left(\frac{\lambda_{eff}}{c_p}gradT\right)+s_T \tag{8}$$

The continuity equation:

$$\frac{\partial \rho}{\partial t}+u\frac{\partial(\rho u)}{\partial x}+v\frac{\partial(\rho v)}{\partial y}+v\frac{\partial(\rho w)}{\partial z}=0 \tag{9}$$

NS equations:

$$\rho\frac{d\vec{V}}{dt}=\rho\vec{F}-grad\,\vec{P}+\mu\nabla^2\vec{v} \tag{10}$$

Differential equations for thermal conductivity:

$$\frac{\partial T}{\partial \tau}=a\nabla^2 T+\frac{q_v}{cp} \tag{11}$$

Boundary conditions:

$$\left.\frac{\partial T}{\partial y}\right|_{y=y_d}=T_d \tag{12}$$

$$q=h\left(T_w-T_f\right) \tag{13}$$

$$h_{y=y_t}=8 \tag{14}$$

2.3.2 Infrared image pre-processing

Prior to the analysis of the infrared thermal imaging images, denoising processing needs to be carried out first because infrared thermal imaging cameras are vulnerable to the reflection effects caused by the surface of the steam pipelines, uneven emissivity, environmental factors

and other interference in the process of data acquisition, which will lead to the presence of noise in the captured infrared thermal imaging image, making the defective information is not obvious, and thus the thermal imaging images need to undergo denoising processes using the non-local mean filtering method. The non-local mean filtering method is an image denoising technique which does not confine itself to focusing on the immediate locality of each pixel in the image, but also utilizes the information of the whole image to remove the noise. But the fundamental concept behind the denoising method is to select a window of a certain size which encompasses a section of the image around the pixel being processed. Next, the method involves searching for similar blocks of content across the entire image to the selected window, The similarity metric is usually measured using mean square deviation or other distance metrics. Whereafter the method calculates the mean values of the similar blocks and replaces the pixel value with the calculated mean value of the blocks containing the same image content, such that similar pixels in the image will replace the existing pixel value with a weighted average.

2.3.3 SVM defect classification

Steam pipeline leakage detection is essentially an image multi-classification problem, and the key lies in identifying whether there are temperature field anomalies in the images detected by infrared thermal imaging sensors, i.e., determining the image with leakage (Label 1), the image without leakage (Label 2), and then determining the image region corresponding to the leakage point. The SVM classifier from the field of machine learning is used in this thesis as the tool for the classification and recognition of images from the steam pipes that have defects. In this respect, the SVM classifier eliminates the disadvantages of using linear classifiers by the implementation of the concept of dual space; this makes it possible to map feature vectors into the high dimensional space according to the principles of structural risk minimization, and then complete the task of classifying the data in this space. The core of steam pipe leakage detection based on SVM model is to construct an efficient classifier. First, we need to design a classifier with good performance; then, load the image feature data according to the input requirements; then, then this data is used to train the classifier, and through further optimization processes, the final optimal model of the classifier is created. The main stages involved in this case are the extraction of the features, choosing the proper kernel function, training, and parameter tuning.

3 Gas power plant intelligent inspection integration platform application simulation analysis

3.1 Oil Leak Detection

There is no authoritative public dataset for pipeline leakage images in power plants, and it is difficult to collect image data of leakage occurring in pipelines of actual power plants, so there is no pipeline leakage image dataset that can be directly utilized. Through field visits to power plants and pipeline leakage scenario simulation experiments, as well as synthesizing the existing leakage images and video data in power plants, this paper constructs an oil leakage detection dataset for pipelines in key areas of power plants, which covers indoor and outdoor pipelines, valves and other scenarios. A large amount of data was collected in the form of videos and pictures, and finally, through data cleaning, a total of 5000 pipeline oil leakage images were retained for the construction of the dataset, the image data set was split randomly into training, validation, and test sets in the ratios of 80%, 10%, and 10%, respectively, by means of script files in Python language.

3.1.1 Comparative experiments

In order to make a fair comparison on the performance of the proposed improved algorithm for YOLOv5, some popular algorithms for target detection will be tested using the self-built data set for pipeline oil leakage detection under the same experimental environment. As shown in Table 1, it can be seen that the improved algorithm has the highest accuracy rate in detecting the pipeline oil leakage among the tested algorithms, outperforming Mask R-CNN, which is the second-best performing algorithm, by 16.62%. And the improved algorithm also improves in speed, compared with other YOLO series of target detection algorithms there is an improvement of 3~5 frames, compared with other algorithms the speed improvement is more obvious.

Table 1: Performance comparison of different algorithms

Algorithm	mAP/%	FPS
SSD	49.27	35
Mask R-CNN	63.52	12
CenterNet	54.66	29
YOLOv2	56.15	25
YOLOv4	59.23	27
YOLOv5s	61.96	26
The proposed	80.14	30

3.1.2 Ablation experiments

In this study, some improvement strategies have been proposed for the backbone network, feature fusion block, and loss function of the initial YOLOv5s model. In order to measure the influence of each separate improvement strategy and combinations of different improvements on the final performance of the algorithm, we perform ablation tests. The experiment results are summarized in Table 2. From the experimental results, it is observed that each improvement strategy separately leads to a positive impact on the final performance of the algorithm, and the most outstanding one is the Focal EIoU Loss, which improves the accuracy of the recognition. Additionally, a combination of different improvements can also positively affect the final performance of the algorithm. The most optimized result of the combination of the three improvement strategies reaches the mean average precision of 80.14%.

Table 2: Results of ablation experiments

Algorithm	Recall	Precision	mAP/%
YOLOv5	55.23	56.82	56.01
YOLOv5+CBAM	57.38	62.17	59.68
YOLOv5+BiFPN	64.59	65.44	65.01
YOLOv5+Focal Loss	67.94	66.78	67.36
YOLOv5+CBAM+BiFPN	68.12	69.63	68.87
YOLOv5+BiFPN+Focal Loss	74.98	75.56	75.27
YOLOv5+CBAM+Focal Loss	75.32	76.77	76.04
The proposed	79.73	80.56	80.14

3.1.3 Analysis of test results

(1) Analysis of pipeline single leak detection results

The P-R curve comparison for the detection of a single leakage point using the same self-built pipeline dataset is provided in Figure 6 below, by comparing it to other YOLO series target

detection methods. Through the comparison result, it can be observed that the optimized YOLOv5 method designed in this paper obtains the largest area under the P-R curve and has the highest mean average precision of 98.22%.

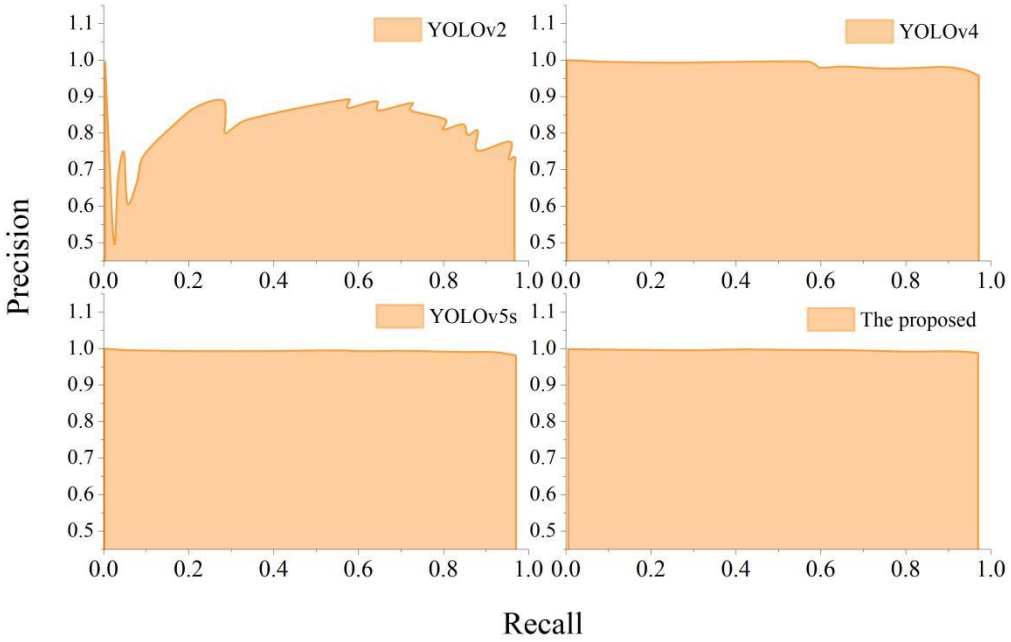

Figure 6: P-R curves for detection of a single leak point in the pipeline

(2) Analysis of pipeline multi-leakage point detection results

A similar comparison is performed using a multi-leakage point dataset with the same detection environment, and its P-R curves are illustrated in Figure 7 below. In the case of multi-leakage point detection, the optimized YOLOv5 method still obtains the largest area under the P-R curve, and the highest mean average precision of 97.96% is obtained.

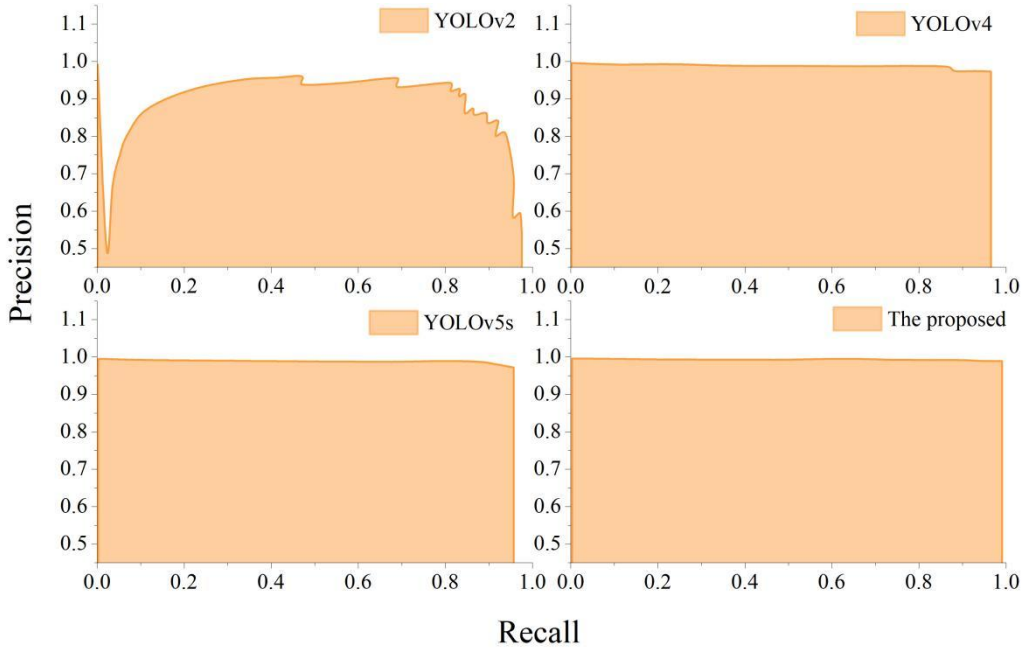

Figure 7: P-R curves for detection of multiple leakage points in pipelines

3.2 Vapor Leak Detection

A steam generator was selected as the source of water vapor preparation and a bath light as the radiant heating source. The leaky parts were machined by drilling step holes to simulate real leaks. In this section, practical experimental verification is carried out by processing artificial leak holes and false leaks, and the feasibility of dynamic and accurate determination of leak parts is demonstrated by using telemetric sensing of leak parts and studying the remote realization of pressure testing of pressurized equipment by on-site personnel.

3.2.1 Feasibility verification of infrared thermography for leak detection

Through the numerical simulation of the steam leakage process, it is obtained that when the steam leakage occurs, the real temperature of the outer surface at the leakage point will be higher than that of the outer surface at the non-leakage point, but the temperature difference is not very obvious, which is likely to lead to the temperature anomalies at the leakage point being submerged in the measurement error in the background of the temperature measurement of the infrared thermal imaging camera. Therefore, this paper proposes to increase the radiation temperature difference between the leakage point and the non-leakage point based on the high radiation temperature contrast caused by the difference between the emissivity of the small droplets and the surface of the pressurized equipment material, as well as the radiation temperature difference caused by the higher real temperature of the wall at the leakage point than that at the non-leakage point.

The results of the temperature distribution by the infrared thermal imager on the surface of the target to be measured are shown in Fig. 8. The leakage point has a unique superheated infrared characteristics, in order to better analyze the characteristics of the radiation temperature distribution at the leakage point, the detected infrared thermal imaging map of the local zoom processing, can be clearly presented at the leakage point of the superheated infrared characteristics, the maximum radiation temperature difference reaches more than 15k, much higher than the results of the numerical simulation. Through the real temperature measurement by contact thermocouple, the real temperature difference between the leakage point and the non-leakage point is less than 1 K. After the steam leakage, the small liquid droplets attached to the outer surface of the leakage point, and the difference in emissivity of the metal wall leads to a larger radiation temperature difference, which is superposed on top of the real temperature difference, realizing the goal of increasing the temperature difference between the leakage point and the non-leakage point. Therefore, it is feasible to apply infrared thermography to leak detection of pressurized equipment.

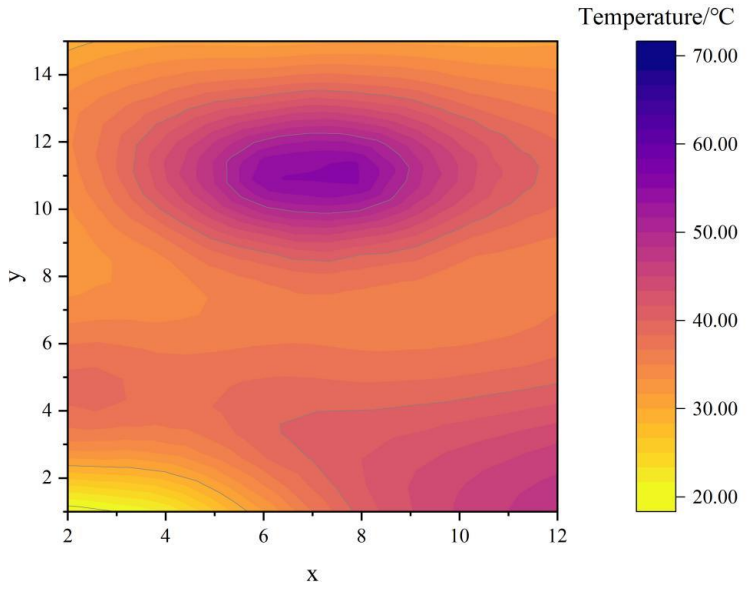

Figure 8: Results of temperature distribution

In order to better investigate the features of the radiation temperature field at the leakage position, the radiation temperature field along the vertical axis of the target surface through the leakage position is considered as the object of analysis. The changing feature of the radiation temperature field at the leakage position on the outer wall surface is illustrated in Fig. 9. With the steam leakage time of 20 seconds, the temperature deviation from the leakage position is still rather subtle, and with the passage of time, the overheating characteristics at the leakage point become more and more obvious, and the radiation temperature difference between the leakage point and the non-leakage place reaches more than 15K. Therefore, in the process of steam leakage, real-time monitoring of the radiation temperature distribution on the external surface by infrared thermal imager can realize the rapid capture of the leakage point.

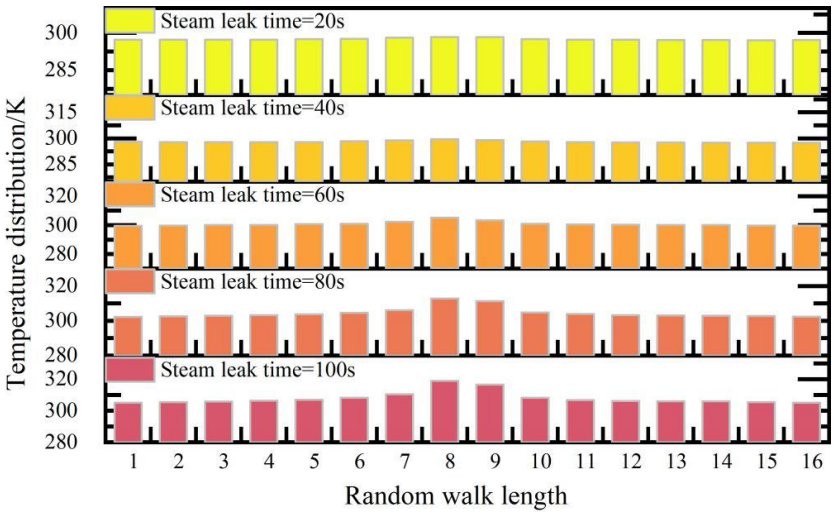

Figure 9: Variation of radiation temperature distribution with time

3.2.2 Analysis of test results

Given that the practical application of the detection process does not necessarily guarantee a perpendicular position concerning the leakage site, and to make sure that the detection process becomes adaptable to different situations, the following experiment utilizes two positions of

detection: one perpendicular to the target area and another at a 20-degree deviation from the perpendicular position. For the purpose of conducting this experiment, steam is generated by a steam generator and is directed to the point of leakage through a pipeline that is connected to the steam generator through tees and elbows.

(1) Normal to the target surface detection

Verify the leak detection model, in the temperature is approximately the same, high temperature water vapor heating and radiant heating source heating radiation temperature dot matrix subtraction results shown in Figure 10. With the help of MATLAB radiation temperature point array subtraction, the output of the isothermal distribution of the entire target surface, the two heating methods in the real temperature is nearly the same under the surface emissivity is considered to be the same, the image processing, the false leakage point A, B to eliminate the impact of the radiation temperature of the infrared characteristics of the disappearance of the higher temperature, while the real leakage point C at the overheating of the infrared characteristics of the infrared characteristics are still obvious, showing a different from the false leakage point of the exclusive infrared thermal characteristics, thus eliminating the detection interference due to the different emissivity, and from the isothermal distribution at the leakage point C, it can be found that after the leakage modeling process, the radiation temperature gradient has increased significantly.

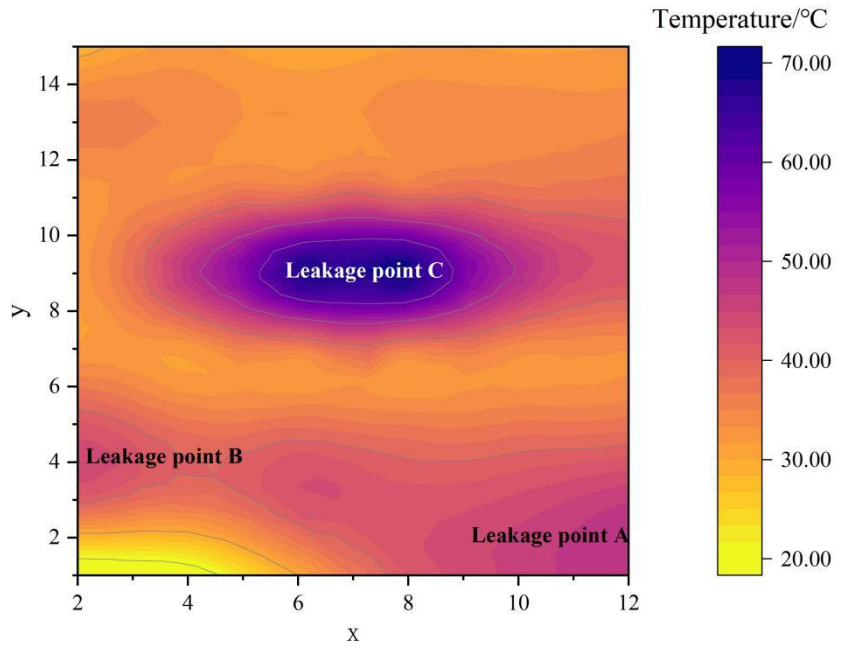

Figure 10: Treatment results of temperature distribution

(2) Detection at an angle of 20 degrees from the normal clip

With the normal clip 20 degrees angle position arrangement of infrared thermal imager, according to the detection step detection, the image radiation temperature dot matrix subtraction processing, temperature distribution processing results shown in Figure 11. Each thermal imaging image to do radiation temperature dot matrix subtraction processing, when the temperature of the two heating methods is approximately the same, the value of the temperature of the surface area of the non-leakage fluctuations in the vicinity of 15 ℃, due to the high emissivity caused by the false leakage of A, B interference is eliminated, only the real leakage of the infrared characteristics of the high radiation temperature of the point C, and then you can accurately determine whether the leakage occurs.

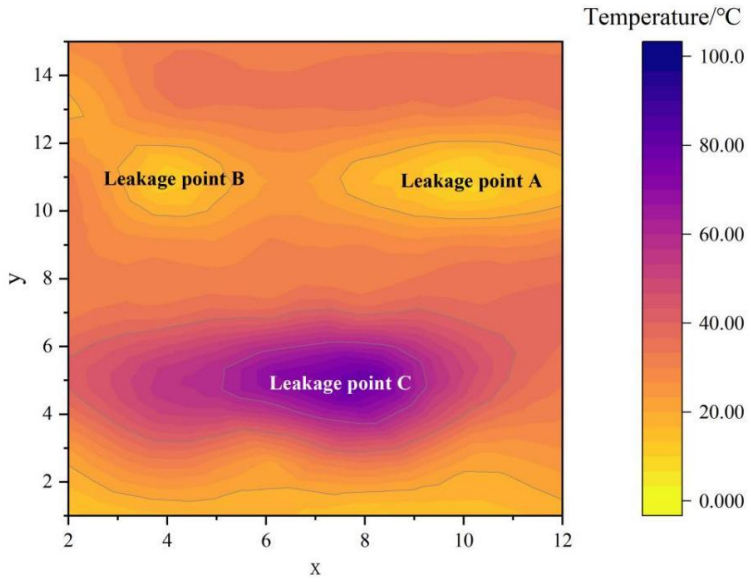

Figure 11: Treatment results of temperature distribution

We collect multiple steam leakage experimental data captured by infrared camera and build our own dataset to carry out performance testing experiments. When there is no need for leakage level judgment, and only do the dichotomous discrimination between leakage and no leakage, this paper defines the sample size of no leakage but predicted to be leakage than on the real leakage sample size as the false alarm rate of leakage, and the value of the predicted real leakage sample size compared to on the real labeled leakage is the alarm rate of leakage, and the closer the value is to 1 the better it is, and it can be greater than 100%. The detection results of different algorithms are shown in Table 3. In this paper, we use the algorithm leakage alarm rate closest to 1, the best detection effect.LSBP algorithm is more sensitive, exceeding 100%, more false alarms.GMG algorithm has the worst recognition effect for this scenario, only 12.45% alarm rate. Accuracy and recall are both dichotomous indicators, when used for multi-classification, this paper according to the proportion of samples in the total samples for the four classes of results to assign weights to take the weighted average to get the corresponding indicators, it can be seen that the detection of each leakage class class i has different feature thresholds, resulting in other algorithms of the F1 indicators with i (i=1,2,3) class precision rate is not high, coupled with the imbalance of the samples of each class, it will occur take the value of 0 as a result. However, the steam leakage problem is most concerned with leakage or not, i.e., dichotomous problem, it can be seen that the algorithms in this paper and other algorithms perform better in terms of leakage alarm rate and false alarm rate, except for GMG algorithm which can reach more than 90%, and the false alarm rate is less than 3%.

Table 3: Detection results of different algorithms(%)

	LSBP	GMG	CNT	The proposed
Leakage alarm rate	102.57	12.45	94.25	99.13
Leak false alarm rate	2.57	0.00	0.00	0.00
Precision	18.48	93.01	28.74	93.56
Recall	20.18	8.37	49.17	92.55
F1	19.29	15.36	36.28	93.05
Type 1 accuracy	49.66	0.00	0.00	47.27
Type 2 accuracy	3.15	68.38	54.12	91.59
Type 3 accuracy	17.37	0.00	0.00	99.02

4 Conclusion

In consideration of the function requirements for intelligent inspection in gas power plants, an optimized YOLOv5 detection algorithm is combined with infrared thermal imaging technology to accomplish accurate oil and steam leakages. Based on a comprehensive experimental study with different scenarios, the feasibility of the proposed method was analyzed via experimental test results and simulation tests on the designed samples.

(1) In terms of the self-created dataset, the detection accuracy of the improved YOLOv5 algorithm can reach up to 80.14%, while the algorithm can also achieve 3-5 FPS enhancement compared with the state-of-the-art methods like YOLO series. According to ablation studies, applying three optimizations simultaneously can produce the most effective results among all the examined algorithms, with the highest mAP in both single and multiple leakages detection scenarios.

(2) The results of normal and tilt detection show that this method can eliminate the interference of false leaks and retain only the overheating characteristics of real leaks with a significant increase in temperature gradient. The steam leakage alarm rate is close to 1 and the false alarm rate is 0, which is better than the comparative algorithms such as LSBP.

This paper's platform is able to efficiently detect pipeline leaks and defects in gas power plants in complex environments, providing feasible technical support and realization paths for the safety monitoring of smart power plants.

About the Author

Zhimin Cui was born in Baoding, Hebei in 1972. He graduated from Tianjin University and obtained a double bachelor's degree in Applied Chemistry and Industrial Management Engineering. He is committed to the intelligent construction and management of power plants.

References

[1] Tiwari, S., Khan, S., Mohammed, K. S., & Bilan, Y. (2024). Connectedness between artificial intelligence, clean energy, and conventional energy markets: Fresh findings from CQ and WLMC techniques. Gondwana Research, 136, 92-103.

[2] Qiao, Z., Guo, Q., Sun, H., & Sheng, T. (2018). Multi-time period optimized configuration and scheduling of gas storage in gas-fired power plants. Applied Energy, 226, 924-934.

[3] Qureshi, Y., Ali, U., & Sher, F. (2021). Part load operation of natural gas fired power plant with CO2 capture system for selective exhaust gas recirculation. Applied Thermal Engineering, 190, 116808.

[4] Wang, G., Bi, M., Fan, H., Fan, Y., Huang, C., Shi, Y., ... & Hua, H. (2023). Key problems of gas-fired power plants participating in peak load regulation: A review. IET Cyber-Physical Systems: Theory & Applications, 8(4), 222-235.

[5] Elias, R. S., Wahab, M. I. M., & Fang, L. (2018). Retrofitting carbon capture and storage to natural gas-fired power plants: A real-options approach. Journal of Cleaner Production, 192, 722-734.

[6] Meng, F., & Dillingham, G. (2018). Life cycle analysis of natural gas-fired distributed combined heat and power versus centralized power plant. Energy & Fuels, 32(11), 11731-11741.

[7] Glensk, B., & Madlener, R. (2019). The value of enhanced flexibility of gas-fired power plants: A real options analysis. Applied energy, 251, 113125.

[8] Gatti, M., Martelli, E., Di Bona, D., Gabba, M., Scaccabarozzi, R., Spinelli, M., ... & Consonni, S. (2020). Preliminary performance and cost evaluation of four alternative technologies for post-combustion CO2 capture in natural gas-fired power plants. Energies, 13(3), 543.

[9] ROY, B., GANGULY, S., & CHATTOPADHYAY, S. (2018). Managing major shutdown and maintenance of large sized gas fired combined cycle power plant: a journey towards excellence. Indian Journal of Power & River Valley Development, 68.

[10] Onen, P. S., Zubo, R. H., Ali, N. T., Mokryani, G., Li, J. P., & Abd-Alhameed, R. (2024). Stochastic Expansion planning Model for a coordinated Natural gas and Electricity Networks Coupled with Gas-fired Generators, Power-to-Gas Facilities and Renewable Power. IEEE Access.

[11] Madejski, P., Żymełka, P., Węzik, R., & Kubiczek, H. (2017). Gas fired plant modeling for monitoring and optimization of electricity and heat production. Journal of Power Technologies, 97(5), 455-462.

[12] Khalid, S., Lim, W., Kim, H. S., Oh, Y. T., Youn, B. D., Kim, H. S., & Bae, Y. C. (2020). Intelligent steam power plant boiler waterwall tube leakage detection via machine learning-based optimal sensor selection. Sensors, 20(21), 6356.

[13] Ma, X., Lv, T., Jin, Y., Chen, R., Dong, D., & Jia, Y. (2021). Cloud based monitoring and diagnosis of gas turbine generator based on unsupervised learning. Energy Engineering: Journal of the Association of Energy Engineers, 118(3), 691.

[14] Akhtar, M., Kamran, M. S., Hayat, N., Rehman, A. U., & Khan, A. A. (2021). High-vibration diagnosis of gas turbines: An experimental investigation. Journal of Vibration and Control, 27(1-2), 3-17.

[15] Bunyan, S. T., Khan, Z. H., Al-Haddad, L. A., Dhahad, H. A., Al-Karkhi, M. I., Ogaili, A. A. F., & Al-Sharify, Z. T. (2025). Intelligent Thermal Condition Monitoring for Predictive Maintenance of Gas Turbines Using Machine Learning. Machines, 13(5), 401.